ChemComm

COMMUNICATION

View Article Online
View Journal | View Issue

Cite this: *Chem. Commun.*, 2016, 52, 1513

Received 11th November 2015,
Accepted 26th November 2015

DOI: 10.1039/c5cc09361a

www.rsc.org/chemcomm

Water oxidation catalysis: an amorphous quaternary Ba-Sr-Co-Fe oxide as a promising electrocatalyst for the oxygen-evolution reaction†

Cuijuan Zhang,‡[a] Curtis P. Berlinguette[ab] and Simon Trudel*[a]

We present an amorphous quaternary Ba-Sr-Co-Fe oxide (a-BSCF) with a specific stoichiometry, readily fabricated *via* a photochemical decomposition method. a-BSCF demonstrates high catalytic activity towards the oxygen-evolution reaction (OER).

Water oxidation is the focus of significant interest and recent efforts due to its potential application in the storage of intermittent renewable energy sources (*e.g.* solar, wind, and tidal) in the form of a chemical fuel, namely hydrogen.[1,2] Furthermore, the development of novel catalysts for the water-oxidation reaction can shed light on the development of catalysts for related energy-intensive small-molecule transformations, including *e.g.* carbon monoxide oxidation, methanol and ethanol oxidation, and metal–air batteries.[3–6] To this day, the high overpotential required for the oxygen-evolution reaction (OER) – due to the four-proton and four-electron transfers – significantly impedes the commercial viability of water electrolysis. Therefore, developing highly active and stable OER catalysts while maintaining low cost is greatly desirable to enhance the efficiency of this process and reduce the cost of hydrogen-fuel production. Among the noble-metal-free metal oxides,[7–12] perovskite materials, *e.g.* $LaNiO_3$,[13–16] $LaCoO_3$[13,14,17] $La_{1-x}Ca_xCoO_{3-\delta}$,[18] and $La_{1-x}Sr_xCo_{1-y}Fe_yO_{3-\delta}$,[19] deliver promising electrocatalytic activity towards the OER. In all cases, multi-metal oxides are employed, strengthening the case that composition control is key to preparing superior catalysts.

The activity of an electrocatalyst is determined by geometric and electronic factors,[8,9,20,21] such as surface area and concentration of active sites for the former, and the electronic structure and nature of the active site for the latter. Efforts have been ongoing to study the influence of these various factors on the electrocatalytic activity.[8,9,12–14,17,20,22] Suntivich *et al.* studied the relationship between OER activity and the occupancy of 3d electrons in states with e_g symmetry of surface transition metal cations in an oxide, and out of a series of perovskite OER catalysts found that the intrinsic OER activity of $Ba_{0.5}Sr_{0.5}Co_{0.8}Fe_{0.2}O_{3-\delta}$, with an e_g occupancy close to unity, is more than one order of magnitude higher than that of the state-of-the art iridium oxide in alkaline media.[23] Beyond being an excellent catalyst for the oxygen-reduction reaction,[24,25] $Ba_{0.5}Sr_{0.5}Co_{0.8}Fe_{0.2}O_{3-\delta}$ is also a highly active and promising OER catalyst. Importantly, May *et al.* found that the activity of $Ba_{0.5}Sr_{0.5}Co_{0.8}Fe_{0.2}O_{3-\delta}$ increased with electrochemical cycling, possibly due to the amorphization of surface layers.[26] This suggests that amorphous $Ba_{0.5}Sr_{0.5}Co_{0.8}Fe_{0.2}O_{3-\delta}$ is a candidate high-activity OER catalyst. However, to date no viable method to access quaternary amorphous metal oxides with controlled composition has been reported.

We recently reported that photochemical deposition is a simple and scalable process to prepare superior amorphous metal-oxide (single, binary, and ternary metal oxides) OER catalysts.[27–31] Herein, photochemical deposition is extended to the preparation of an amorphous quaternary metal oxide comprising Ba, Sr, Co, and Fe, demonstrating for the first time the rational and controlled preparation of an amorphous quaternary OER catalyst. The amorphous Ba-Sr-Co-Fe oxide exhibits significantly higher activity towards the OER compared to its crystalline counterpart, emphasizing the usefulness of this approach, and the unique benefit its ability to prepare elaborate OER catalysts affords.

Amorphous $Ba_{0.5}Sr_{0.5}Co_{0.8}Fe_{0.2}O_{3-\delta}$ (a-BSCF) is prepared by a photochemical deposition protocol[27,32,33] using metal 2-ethylhexanoate precursors.† The metal precursors were dissolved in hexanes in the desired stoichiometric ratio with a total precursor concentration of 15% w/w. This precursor solution was spin-coated onto cleaned fluorine-doped tin oxide (FTO) substrates and then subjected to deep-UV light irradiation.

[a] *Department of Chemistry and Centre for Advanced Solar Materials, University of Calgary, 2500 University Dr NW, Calgary, AB, Canada T2N 1N4. E-mail: trudels@ucalgary.ca; Fax: +1-403-289-9488; Tel: +1-403-210-7078*

[b] *Departments of Chemistry and Chemical & Biological Engineering, The University of British Columbia, 2026 Main Mall, Vancouver, BC, Canada V6K 1Z6*

† Electronic supplementary information (ESI) available: Experimental details, XPS results, SEM images and elemental mapping, XRD, FTIR, and stability testing. See DOI: 10.1039/c5cc09361a

‡ Present address: Department of Mechanical Engineering, University of South Carolina, Columbia, SC, USA.

The disappearance of infrared absorption bands from the precursors' coordinated ligand (Fig. S1†) over a 12 h period indicates that the ligand is photolysed; new bands are attributed to surface carbonate ions†[34] as was documented in our study of amorphous lanthanum-transition metal binary oxides.[30] The microstructure of the resultant film on the FTO substrate as seen from scanning electron microscopy (SEM) shows a smooth and featureless film with good coverage of the FTO substrate (Fig. S2†). Energy-dispersive X-ray spectroscopy elemental mapping of the a-BSCF film (Fig. S3†) demonstrates that the four metal elements are uniformly distributed within the film, without segregation or local enrichment. Inductively-coupled plasma optical emission spectroscopy (ICP-OES) confirmed an actual film composition of $Ba_{0.55}Sr_{0.45}Co_{0.77}Fe_{0.23}O_x$, in excellent agreement with the nominal composition of $Ba_{0.5}Sr_{0.5}Co_{0.8}Fe_{0.2}O_{3-\delta}$. These results show that photochemical depostion is a reliable process to fabricate homogeneous quaternary oxides with precisely controlled composition.

The amorphous nature of the film was confirmed by X-ray diffraction (XRD); only Bragg reflections expected from the crystalline FTO substrate are observed, indicating that X-ray amorphous films are obtained (Fig. S4†). This finding is consistent with previous XRD,[27,30] transmission electron microscopy,[31] extended X-ray absorption fine structure spectroscopy,[33] and atomic pair-distribution function analysis of high-energy X-ray scattering data[35] which indicate that the photochemical deposition process yields amorphous films.

The oxidation states of the constituent metals at the film surface in an as-prepared a-BSCF film were probed using X-ray photoelectron spectroscopy (XPS). Two Ba^{2+} species are evidenced from $3d_{5/2}$ binding energies of 780.0 and 781.4 eV,§ which are ascribed to oxide and carbonate species, respectively (see Fig. S5 and Table S1†).[36–38] The presence of a carbonate species is expected from the FTIR results presented above. The spectrum collected in the Sr 3d region is consistent with the spin–orbit coupled doublet expected for a Sr^{2+} oxide species such as SrO (Sr $3d_{5/2}$ at 133.4 eV; Sr $3d_{3/2}$ at 135.1 eV). The cobalt is primarily attributed to a cobalt(II) oxide species (Co $2p_{3/2}$ at 780.0 eV; Co $2p_{1/2}$ at 795.4 eV; 96.5% relative area of the Co signal) with a minor cobalt(II) hydroxide species accounting for the remainder of the signal (Co $2p_{3/2}$ at 781.9; Co $2p_{1/2}$ 797.3 eV).[38] The XPS signal for the iron species is rather complex, but appears to be attributable to trivalent iron oxide and oxyhydroxide species.[27] Three species adequately fit the envelope of the O 1s spectrum, which are assigned to oxygen in the form of oxide ions O^{2-} in metal-oxygen bonds (529.4 eV), and adsorbed CO_3^{2-} (531.1 eV) and OH^- (532.4 eV), respectively.[38]

The metal oxidation states can also be inferred from cyclic voltammetry (CV) measurements. Fig. 1a shows the CVs of a-BSCF after the first, second, and sixth cycles. During the first cycle, an apparent oxidation peak $E_{p,a}$ at 1.08 V *vs.* RHE is observed. In the second and subsequent cycles, $E_{p,a}$ decreases to 1.01 V with decreased oxidation current density. As the XPS result reveals the presence of $Co^{II}O$ and $Co^{II}(OH)_2$, the oxidation peaks at 1.08 and 1.01 V are attributed to the oxidation of CoO and $Co(OH)_2$ to $Co^{III}OOH$. The OER catalytic current starts

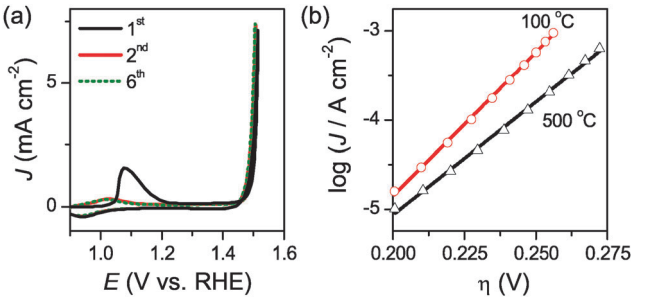

Fig. 1 (a) CVs and (b) Tafel plot for a-BSCF in 0.1 M KOH at a scan rate of 10 mV s^{-1}. The Tafel plot of a film annealed at 500 °C is also shown for comparison. Lines in (b) are a linear fit to the data.

at *ca.* 1.46 V and increases sharply with increasing potential. Although the coexistence of Co(III) and Co(IV) under anodic conditions (evidenced from *in situ* Mössbauer[39] and X-ray absorption near-edge structure spectroscopies[40]) has been previously reported for cobalt oxides, no obvious oxidation peak related to Co(III/IV) is observed; this feature is likely masked by the OER catalytic wave. The catalytic current density slightly increased from the first to the second cycle and then remained constant. The reduction peak potential is the same for all the cycles, 0.96 V, attributed to the reduction of $Co^{III}OOH$ to $Co^{II}(OH)_2$.[28]

Steady-state measurements in the Tafel regime were performed to further evaluate the electrode kinetics of a-BSCF towards the OER (Fig. 1b). The attained Tafel parameters in terms of Tafel slope, the onset overpotential of catalysis, and the overpotentials required to achieve current densities of 0.05 and 1 mA cm^{-2} are listed in Fig. 2. The Tafel parameters for the films annealed at 500 °C for 1 h and the reported results for crystalline $Ba_{0.5}Sr_{0.5}Co_{0.8}Fe_{0.2}O_{3-\delta}$[23] are also listed for comparison. The a-BSCF film annealed at lower temperature outperforms both the sample annealed at 500 °C and the reported crystalline material with the same composition.[23] Compared with the latter crystalline material, the Tafel slope and η @ 0.05 mA cm^{-2} of a-BSCF are lower by *ca.* 20 and 40 mV, respectively. The current density at the same overpotential (~0.25 V) increases by a factor of *ca.* 20 for the present a-BSCF film, taking caution to specify that these current densities are related to geometric, not real, surface areas. Furthermore, the activity of a-BSCF (30 ± 2 mV dec^{-1}, 0.252 ± 0.004 V @ 1 mA cm^{-2}) is remarkably higher than that of

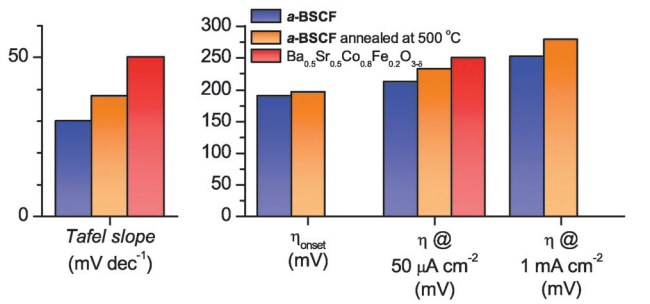

Fig. 2 Kinetic parameters for a-BSCF, an a-BCSF film annealed at 500 °C, and $Ba_{0.5}Sr_{0.5}Co_{0.8}Fe_{0.2}O_{3-\delta}$.[23]

the state-of-the-art crystalline IrO_x (49 ± 1 mV dec^{-1}, 378 ± 4 mV @ 1 mA cm^{-2}).[12] In addition, a-BSCF demonstrates significantly higher electrocatalytic performance towards the OER than the reported typical perovskite oxides, *e.g.* $LaNiO_3$ (42 mV dec^{-1},[16] 0.32 V @ 0.05 mA cm^{-2}),[23] $LaCoO_3$ (70 mV dec^{-1},[13] 0.32 V @ 0.05 mA cm^{-2}),[23] and $La_{0.6}Ca_{0.4}CoO_3$ (55–60 mV dec^{-1}).[18] Collectively, these results demonstrate the superior electrocatalytic activity of a-BSCF towards the OER. We ascribe this performance to the presence of a larger number of coordinately unsaturated surface metal sites available for reaction, and the isotropic and single-phase nature of amorphous materials.[41] We also hypothesize that similar trends correlated with e_g occupancy may be present;[23] verifying this assertion will be the focus of future work.

To gain further insight into the processes occurring during the OER, electrochemical impedance spectroscopy was carried out on the films after Tafel measurements. The typical impedance spectra of a-BSCF at various applied potentials are presented in Fig. 3a and b. All spectra are composed of two semi-circles, which are well fit with the equivalent circuit presented in Fig. 3c, where R_s is the solution resistance (*i.e.*, the intercept of the highest frequency with the abscissa axis); Q_{film} and R_{film} are related to the dielectric properties and resistivity of the film; Q_{dl} and R_{ct} are the double-layer capacitance and the interfacial charge-transfer resistance, respectively.[42] R_s (not shown) and R_{film} (Fig. 3d) remain constant over the applied potential range studied here, whilst R_{ct} decreased with increasing applied potential, consistent with the rapid increase of current density after the onset potential (Fig. 1). The resistance of the film is higher than the charge-transfer resistance at applied potentials greater than 1.50 V *vs.* RHE, and thus becomes the dominating resistance; this result infers that increasing the electrical conductivity of this material would further enhance the electrocatalytic activity of a-BSCF towards the OER.

Steady-state measurements at different KOH concentrations (*i.e.*, different activities, a_{OH^-}) were carried out to gain further

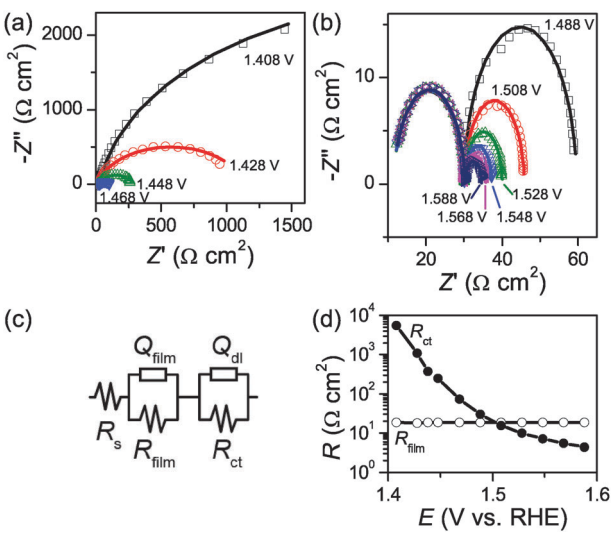

Fig. 3 (a and b) Impedance spectra of a-BSCF film at different potentials (*vs.* RHE) in 0.1 M KOH. The lines in (a and b) are fits using the equivalent circuit shown in (c). (d) Variation of R_{film} and R_{ct} with applied potential.

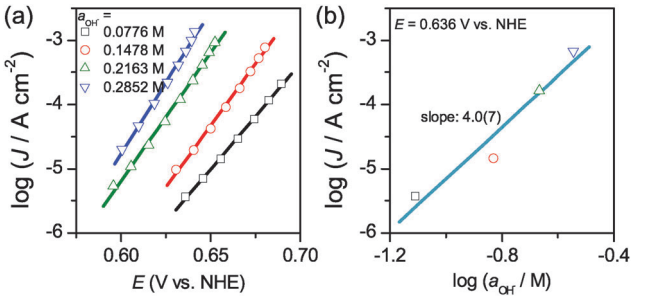

Fig. 4 (a) Tafel plots in KOH solution of different activities. The lines are the linear fit to the data; (b) log$J$ *vs.* loga_{OH^-} at the same potential of 0.636 V *vs.* NHE.

insight into the reaction mechanism. The resultant log$J$ *vs.* E plots are presented in Fig. 4a; the current density J increases with OH^- activity. The reaction order with respect to OH^- was determined to be 4.0 ± 0.7 by fitting the data of Fig. 4b.

A plausible reaction mechanism for the OER[13] on a-BSCF is shown in Fig. 5. While this mechanism involves only cobalt surface sites, iron sites also likely participate in the OER to a lesser extent. Considering the high concentration of coordinately unsaturated surface metal sites expected on the surface of a highly defective amorphous material, high surface coverage θ ($0.2 < \theta < 0.8$) by hydroxide ions is likely. Accordingly, under the conditions of the Temkin isotherm, a Tafel slope of 30 mV dec^{-1} and reaction order with respect to OH^- of 4 are expected, assuming Step 3 of Fig. 5 is the rate-determining step (RDS).[13] The present experimental results (Tafel slope of 30 ± 2 mV dec^{-1}, Fig. 1b; and reaction order of 4.0 ± 0.7, Fig. 4b) are in excellent agreement with this proposed mechanism.[13] This would identify desorption of the hydroxide ion from the surface of a-BSCF film as the RDS. Considering the antibonding character of the d_{z^2} orbital of the 3d metal in M–OH suggested by Bockris and Otagawa,[14] populating the M d_{z^2} orbital would result in weakening of the M–OH bond strength; conversely, the absence of electrons in the d_{z^2} orbital for Co^{4+} suggests strong Co^{IV}–OH binding, hindering the release of OH^- and liberation of oxygen gas.

Finally, the short-term stability of a-BSCF at a constant current density of 1 mA cm^{-2} was evaluated in 0.1 M KOH by chronopotentiometric means. The potential increased by 5.5% at a current density of 1 mA cm^{-2} after 24 h of testing (Fig. S6a, ESI†); meanwhile the Tafel slope increased from

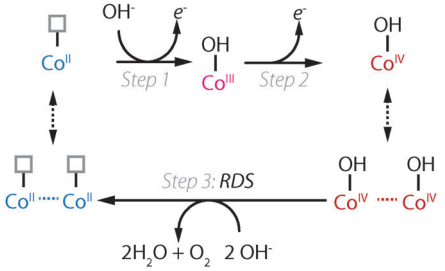

Fig. 5 Proposed OER mechanism on a-BSCF consistent with experimental data.

30.8 to 37.2 mV dec^{-1}, and η @ 1 increased by 13% (Fig. S6b, ESI†). Comparing surface SEM images of the film before and after testing (Fig. S2, ESI†) indicates cracks formed during testing, and a thinning of the catalyst film as the surface roughness of the underlying FTO substrate becomes more apparent. The metal molar ratio of the film after the stability test is found to be 0.80 : 0.20 : 0.75 : 0.25 Ba : Sr : Co : Fe by ICP-OES, indicating preferential dissolution of Sr during testing. Ba, Sr, and Fe were also detected in the electrolyte solution after testing. Accordingly, there is still room to improve the stability of the a-BSCF.

In summary, the amorphous quaternary $Ba_{0.5}Sr_{0.5}Co_{0.8}Fe_{0.2}O_{3-\delta}$ film is first prepared by photochemical deposition and was investigated as an electrocatalyst for the OER. The breakage of the Co^{IV}–OH bond is suggested to be the RDS under Temkin isotherm conditions. The superior activity towards the OER renders the a-BSCF materials a competitive OER catalyst. Importantly, this study demonstrates heeding guidance from the rational design of crystalline high-performance OER catalysts which may be a fruitful approach to the identification of high-performance amorphous OER catalysts. Photochemical deposition is, to the extent of our knowledge, the only method amenable to the controlled formation of such quaternary amorphous metal-oxide OER catalysts.

MITACS and FireWater Fuel Corp. sponsored this project. This research used facilities funded by the University of Calgary and the CFI's John R. Evans Leaders Fund. Dr Shu Yao is thanked for her assistance with XPS data collection.

References

§ All binding energies in this report are calibrated to an adventitious C 1s signal at 284.6 eV.

1 M. G. Walter, E. L. Warren, J. R. McKone, S. W. Boettcher, Q. Mi, E. A. Santori and N. S. Lewis, *Chem. Rev.*, 2011, **111**, 6446.
2 T. R. Cook, D. K. Dogutan, S. Y. Reece, Y. Surendranath, T. S. Teets and D. G. Nocera, *Chem. Rev.*, 2010, **110**, 6474.
3 X. Xie, Y. Li, Z.-Q. Liu, M. Haruta and W. Shen, *Nature*, 2009, **458**, 746.
4 T. Iwasita, *Electrochim. Acta*, 2002, **47**, 3663.
5 C. Xu, Z. Tian, P. Shen and S. P. Jiang, *Electrochim. Acta*, 2008, **53**, 2610.
6 G. Girishkumar, B. McCloskey, A. C. Luntz, S. Swanson and W. Wilcke, *J. Phys. Chem. Lett.*, 2010, **1**, 2193.
7 A. C. C. Tseung and S. Jasem, *Electrochim. Acta*, 1977, **22**, 31.
8 S. Trasatti, *Electrochim. Acta*, 1984, **29**, 1503.
9 P. Rasiyah and A. C. C. Tseung, *J. Electrochem. Soc.*, 1984, **131**, 803.
10 Y. Matsumoto and E. Sato, *Mater. Chem. Phys.*, 1986, **14**, 397.
11 M. Hamdani, R. N. Singh and P. Chartier, *Int. J. Electrochem. Sci.*, 2010, **5**, 556.
12 L. Trotochaud, J. K. Ranney, K. N. Williams and S. W. Boettcher, *J. Am. Chem. Soc.*, 2012, **134**, 17253.
13 J. O. M. Bockris and T. Otagawa, *J. Phys. Chem.*, 1983, **87**, 2960.
14 J. O. M. Bockris and T. Otagawa, *J. Electrochem. Soc.*, 1984, **131**, 290.
15 R. N. Singh, A. N. Jain, S. K. Tiwari, G. Poillerat and P. Chartier, *J. Appl. Electrochem.*, 1995, **25**, 1133.
16 W. G. Hardin, D. A. Slanac, X. Wang, S. Dai, K. P. Johnston and K. J. Stevenson, *J. Phys. Chem. Lett.*, 2013, **4**, 1254.
17 Y. Matsumoto, H. Manabe and E. Sato, *J. Electrochem. Soc.*, 1980, **127**, 811.
18 S. Malkhandi, B. Yang, A. K. Manohar, A. Manivannan, G. K. S. Prakash and S. R. Narayanan, *J. Phys. Chem. Lett.*, 2012, **3**, 967.
19 Y. Matsumoto, S. Yamada, T. Nishida and E. Sato, *J. Electrochem. Soc.*, 1980, **127**, 2360.
20 A. C. C. Tseung and S. Jasem, *Electrochim. Acta*, 1977, **22**, 31.
21 S. Trasatti, *Electrochim. Acta*, 1991, **36**, 225.
22 E. Guerrini and S. Trasatti, *Russ. J. Electrochem.*, 2006, **42**, 1017.
23 J. Suntivich, K. J. May, H. A. Gasteiger, J. B. Goodenough and Y. Shao-Horn, *Science*, 2011, **334**, 1383.
24 Z. Shao and S. Haile, *Nature*, 2004, **431**, 170.
25 Z. Shao, H. Dong, G. Xiong, Y. Gong and W. Yang, *J. Membr. Sci.*, 2001, **183**, 181.
26 K. J. May, C. E. Carlton, K. A. Stoerzinger, M. Risch, J. Suntivich, Y.-L. Lee, A. Grimaud and Y. Shao-Horn, *J. Phys. Chem. Lett.*, 2012, **3**, 3264.
27 R. D. L. Smith, M. S. Prevot, R. D. Fagan, Z. Zhang, P. A. Sedach, M. K. J. Siu, S. Trudel and C. P. Berlinguette, *Science*, 2013, **340**, 60.
28 R. D. L. Smith, M. S. Prevot, R. D. Fagan, S. Trudel and C. P. Berlinguette, *J. Am. Chem. Soc.*, 2013, **135**, 11580.
29 R. D. L. Smith, B. Sporinova, R. D. Fagan, S. Trudel and C. P. Berlinguette, *Chem. Mater.*, 2014, **26**, 1654.
30 C. Zhang, S. Trudel and C. P. Berlinguette, *Eur. J. Inorg. Chem.*, 2014, 660.
31 C. Zhang, R. D. Fagan, R. D. L. Smith, S. A. Moore, C. P. Berlinguette and S. Trudel, *J. Mater. Chem. A*, 2015, **3**, 756.
32 J. P. Bravo-Vasquez, L. W. C. Ching, W. L. Law and R. H. Hill, *J. Photopolym. Sci. Technol.*, 1998, **11**, 589.
33 S. Trudel, E. D. Crozier, R. A. Gordon, P. S. Budnik and R. H. Hill, *J. Solid State Chem.*, 2011, **184**, 1025.
34 S. Bernal, F. J. Botana, R. Garcia and J. M. Rodriguezizquierdo, *React. Solids*, 1987, **4**, 23.
35 J. A. Kurzman, K. E. Dettelbach, A. J. Martinolich, C. P. Berlinguette and J. R. Neilson, *Chem. Mater.*, 2015, **27**, 3462.
36 C. Miot, E. Husson, C. Proust, R. Erre and J. P. Coutures, *J. Mater. Res.*, 1997, **12**, 2388.
37 M. C. B. Lopez, G. Fourlaris, B. Rand and F. L. Riley, *J. Am. Ceram. Soc.*, 1999, **82**, 1777.
38 J. F. Moulder, W. F. Stickle, P. E. Sobol and K. D. Bomben, in *Handbook of X-ray Photoelectron Spectroscopy*, ed. J. Chastain, Perkin-Elmer Corp., USA, 1992.
39 G. W. Simmons, E. Kellerman and H. Leidheiser, *J. Electrochem. Soc.*, 1976, **123**, 1276.
40 M. W. Kanan, J. Yano, Y. Surendranath, M. Dinca, V. K. Yachandra and D. G. Nocera, *J. Am. Chem. Soc.*, 2010, **132**, 13692.
41 C. Yoon and D. L. Cocke, *J. Non-Cryst. Solids*, 1986, **79**, 217.
42 M. E. G. Lyons and M. P. Brandon, *J. Electroanal. Chem.*, 2009, **631**, 62.

